DOI: 10.13009/EUCASS2017-517

Modeling of drop reemission on a small scale rotating Fan model: comparison between experimental and numerical results

C. Laurent, E. Radenac*, B. Déjean*, G. Linassier**, P. Berthoumieu*, J.M. Senoner*, P. Villedieu**
**ONERA – The French Aerospace Lab, F-31055, Toulouse, France*
***SAFRAN Aircraft Engines, F-77550 ,Moissy-Cramayel, France*

Abstract
Within the framework of STORM, a European project dedicated to icing physics in turbojet engines, the runback on rotating blades and the re-emission of droplets at the trailing edge were experimentally and numerically investigated on a small scale rotating Fan model. For this configuration, modelling the reemitted droplet size requires to account for both centrifugal and aerodynamic effects. A coupled model derived from experimental databases dedicated to each effect separately was implemented in ONERA's in house CFD code CEDRE. The simulation of a confined Fan configuration was then performed to validate this model.

1. Introduction

The certification tests for aircraft engines dealing with water ingestion and icing conditions are very difficult to predict due to the complex physical phenomena involved. In this context, the runback on rotating blades and the re-emission of droplets at the trailing edge of blades are studied and models are derived. Indeed, the secondary droplets may impinge further in the engine and lead to ice accumulation and performance degradations. Within the framework of STORM, a European project dedicated to icing physics in turbojet engines, these phenomena have been experimentally and numerically investigated on a small scale rotating Fan model (Figure 1).
Regarding the modeling of the re-emitted droplet characteristics, ONERA first undertook experimental studies on spinning disks. Therefore a model was derived for the droplet size distribution after secondary break-up (Dejean et al. [1]). Comparisons with existing literature were carried out and revealed that the effect of the rim thickness has to be taken into account in order to meet the experimental results at low rotating speed. In this experiment, two main influent parameters were considered, the centrifugal forces and the trailing edge thickness. However, in order to apply this model to turbo-engine simulations, aerodynamic forces need to be considered as well. That is why the droplet re-emission model was enhanced using correlations obtained for pre-filming atomization where centrifugal forces vanish (Chaussonnet et al. [2] model or ONERA model).
In order to validate these experimental correlations when both forces are acting, a small scale rotating Fan model was manufactured. The pressurized injectors used for the experimental campaigns deliver liquid flow rates with the range encountered in Appendix C icing flight conditions. The impinging spray and the re-emitted droplets were characterized with PDA and numerical simulations were performed for validation. The model developed in the STORM context was implemented in the multiphysics ONERA CFD code CEDRE. The droplet atomization at the trailing edge of the Fan is numerically handled by coupling CEDRE's shallow water solver FILM for the runback and CEDRE's Lagrangian solver SPARTE for the droplets. Experimentally, two configurations for the Fan were investigated, an unconfined and a partially confined setup. The droplet size distribution was measured for several liquid flow rates and rotating speeds (Dejean et al. [1]). For the CFD computations, it was found that the gas flow was difficult to simulate: the gas velocity is much lower than in a real Fan and wake vortices appear behind the Fan due to the truncated experimental configuration (see Figure 1). For this reason, the gas flow was only simulated for the partially confined configuration and the analysis and comparisons presented in this paper are focusing on this case.

DOI: 10.13009/EUCASS2017-517

2. The small scale rotating model

2.1 Geometry

The geometry of the Fan was adapted from a real turbomachine, but due to manufacturing and experimental constraints, the blades were truncated at around the mid-height. Additionally, the trailing edge was thickened and one blade out of two removed to improve optical access. Two reduced-scale Fan configurations were investigated, a non-confined and a partially confined configuration (see *Figure 1*). While the former allowed providing droplet measurements upstream and at the tip of the blades, the latter was more representative of a realistic engine.

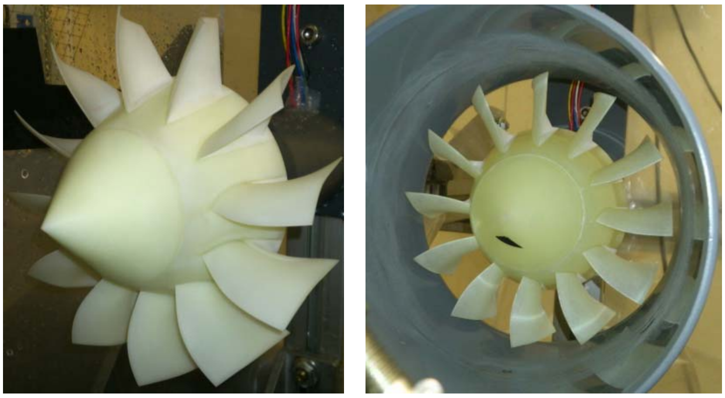

Figure 1: Fan geometry, unconfined and partially confined configurations

2.2 Experimental set-up

The droplet creation is realized by a pressure injector system fed by a pressurized water tank with flowrate controlled ± 0.5 % full scale (same system as for the spinning disk experiment employed to derive the model described in section 3). The injector was positioned 80 mm upstream from the beginning of the blades, which corresponds to 45 mm upstream the cone (Figure 2). The retained liquid flow rates correspond to the icing conditions of aeronautic engines defined by appendix C with liquid water content (LWC) between 0.45 g/m^3 and 1.65 g/m^3 for an airflow impinging a surface equivalent to a 150 mm diameter disk with a velocity of 100 m/s. A parametric study was performed to characterize the influence of rotational velocity and liquid flow rates, as shown in Table 1.

Rotational velocity (rpm)	Liquid flow rate (ml/min)	
0, 1000, 2370	Unconfined	Confined
	50, 100, 175 ml/min	175ml/min

Table 1: Conditions retained for the scaled Fan experiments

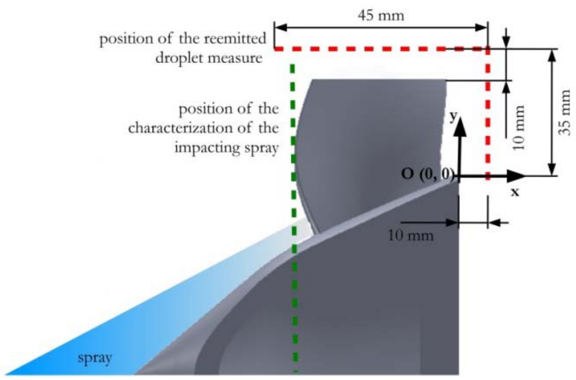

Figure 2: Experimental set-up configuration

DOI: 10.13009/EUCASS2017-517

2.3 Experimental measurements

The Phase Doppler Anemometry (PDA) technique is used to measure droplet size and the droplet velocity distributions while the airflow velocity is measured via Laser Doppler Anemometry (LDA).
Data are available upstream of the Fan in order to provide inlet boundary conditions for the numerical simulations. Concerning the spray characteristics (see Figure 3), only the 175 ml/min injector was used in the partially confined configuration: it is a hollow cone nozzle yielding a droplet size distribution with a Sauter mean diameter D_{32} equal to about 83 µm. Velocity profiles of the gas phase are measured just before the duct which confines the Fan (see Figure 4). The negative radial velocities clearly highlight the aspiration effect of the Fan. As expected, a ratio of two is roughly obtained between the velocity profiles at 1000 rpm and 2370 rpm.
Concerning the data measured downstream, the location of the main measurement planes is shown in Figure 2. In the confined case, results are only available in a plane located 10mm behind the rear wall of the cone (not at the tip of the blade, since there is the shroud). The results will be presented in the following article, in the sections dedicated to the comparisons with numerical results.

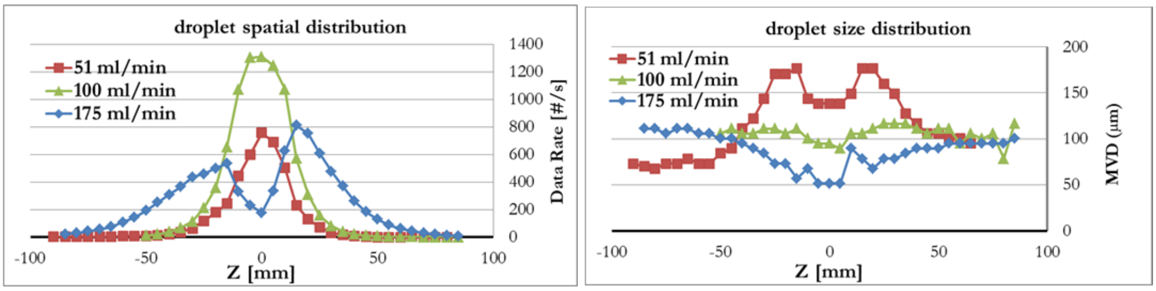

Figure 3: Injector characterization, droplet spatial and size distributions 80mm from injector

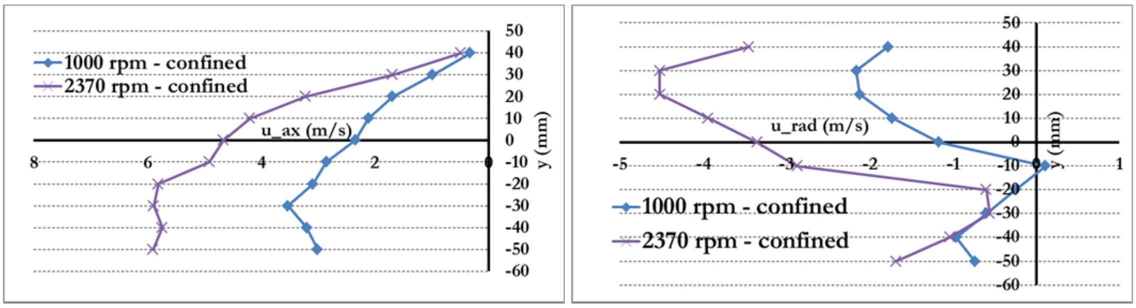

Figure 4: Axial and radial velocity of the airflow upstream of the partially confined Fan, 57mm from the nozzle of the cone.

3. Model for the size of re-emitted droplets

In the case of water ingestion or in icing conditions on protected blades by heating system, runback can occur in engines on blades and then some droplets are re-emitted at the rim of the blades and continue their trajectories in the subsequent rows. Here, the droplet fragmentation is driven by several mechanisms. First, a liquid reservoir is formed at the rim of the blades. Centrifugation then tends to destabilize this liquid volume, leading to the subsequent ejection of droplets. The airflow's shear-stress also contributes to the liquid's destabilization while surface tension acts as the main stabilizing force. In the framework of the STORM project, a model was thus built to account for these three driving phenomena (rim thickness, centrifugation and airflow shear stress). It is based on a Weber number, which balances the destabilizing forces and the surface tension. More details regarding its derivation may be found in Dejean et al. [1]. It is important to note that the model accounts for primary break-up and gives directly the secondary droplet size.
To derive the model, both a spinning disk experiment made in the framework of STORM and a literature review were used. The literature review indicated the presence of several distinct fragmentation regimes for droplet re-emission under centrifugation. Direct drop formation is obtained at the disk's rim for low rotational velocities or low liquid flow rates. When the latter are increased, ligament formation is observed at the disk's rim. These ligaments then break-up into droplets further away from the disk (ligament formation regime). A further increase of rotational velocity and low flow rate leads to the Sheet formation regime, where a liquid sheet is expelled from the disk's rim

DOI: 10.13009/EUCASS2017-517

(Frost, [3]). Numerous correlations were provided for the re-emitted droplet size. They are valid for more or less well identified regimes. Most of them, as well as the transition criteria between regimes, can be expressed as functions of the Weber, Ohnesorge and flow rate numbers:

$$We_D = \frac{\rho_l \omega^2 D^3}{8\sigma_l}, Oh_D = \frac{\mu_l}{\sqrt{\rho_l \sigma_l D}}, V^+ = \frac{\rho_l q^2}{\sigma_l D^3}. \quad \textbf{(1)}$$

In these expressions, D is the disk diameter, ω the disk rotational speed, q the liquid flow rate and ρ_l, σ_l, μ_l the liquid properties, respectively density, surface tension and viscosity. It must be noted that these parameters do not depend on the local characteristics of the film or rivulets at the disk rim. Generally, in the experiments of the literature, the liquid injection on the spinning device was not made by impingement of a spray, but a lot of similarities were observed between the experiments results obtained within the STORM project and the literature. This is consistent with the observation made in STORM that the liquid behaviour on the disk surface has little influence on the droplet re-emission.

Considering the non-dimensional numbers expressed in Eq. (1), which are major parameters of film fragmentation under centrifugation, the range investigated in STORM appears quite different from the conditions expected in a real engine (Table 2). The consequence is that the STORM experiment mainly exhibits Direct Drop and First Ligament regimes of reemission whereas Fully Developed Ligament regime is expected in real engines. The main reason for this discrepancy is the scale reduction, and the difficulty to adjust the liquid properties and engine velocity to retrieve the correct ranges. Moreover, the mean gas velocity is also much lower than expected in a real engine, leading to lower shear stress model. The model derived is thus a priori not fully valid for use in engines. But it has been checked that the model remains consistent with models of the literature addressing higher ranges of We_D and finally Fully Developed Ligament regime. Moreover, in addition to the issue of the reemission regime, the outlet condition is free, which is also different from real Fan conditions. Consequently, the Fan test-case must be considered academic.

Range investigated in	We_D	Oh_D	V^+	Approximate velocity (m/s)
Spinning disk experiment	$1.9\ 10^4$ to $2.3\ 10^6$	$3.0\ 10^{-4}$ to $4.3\ 10^{-4}$	$1.1\ 10^{-5}$ to $9.2\ 10^{-5}$	
Scaled Fan	$8\ 10^4$ to $4\ 10^5$	$3\ 10^{-4}$	$1\ 10^{-5}$ to $3\ 10^{-5}$	10
Realistic engines	$5\ 10^6$ to $2\ 10^9$	$8\ 10^{-5}$ to $2\ 10^{-4}$	$6\ 10^{-5}$ to $1\ 10^{-3}$	100

Table 2: Conditions investigated for the scaled Fan experiments compared to engine conditions

Considering the spinning disk experiment of STORM, a model was derived and compared to the literature for modelling the effect of centrifugation on re-emitted droplets (Dejean et al., [1]). This model has been built to take into account both geometrical, centrifugal and aerodynamic effects by defining characteristic lengths for each phenomenon : h_{te} the trailing edge thickness, $L_a = \frac{\sigma_l}{\tau_p}$ the aerodynamic characteristic length which is the ratio between the stabilizing effect of the surface tension and the destabilizing effect of the gas shear stress and $L_c = \sqrt{\frac{2\sigma_l}{\rho_l D \omega^2}} = \sqrt{\frac{\sigma_l}{\rho_l f_{cent}}}$ the ratio between the surface tension and the centrifugal force. The characteristic length L for the atomization is modelled as an harmonic mean of these different lengths:

$$L = \frac{(1 + K_a + K_c) h_{te} L_a L_c}{K_c h_{te} L_a + K_a h_{te} L_c + L_a L_c} \quad \textbf{(2)}$$

This length is used in the Weber number defined for modelling the mean diameter of the re-emitted droplets:

$$D_{mean} = K \frac{L}{\sqrt{We_L}} \quad \textbf{(3)}$$

which is the general shape of usual correlations for droplet reemission driven by centrifugation. Moreover, Chaussonnet et al. [2] already proposed a similar formula for modeling the primary atomization in a pre-filming configuration, using the trailing edge thickness h_{te} instead of L. The characteristic length model L has been then completed in the framework of STORM to add centrifugal effects. The L_c characteristic length was added in L (see Eq. (2)) and also a new term into the characteristic velocity used in the Weber number:

$$We_L = \frac{\rho_l L u^{*2}}{\sigma_l}, \qquad u^* = \sqrt{\frac{\tau_p}{\rho_g} + \frac{K}{\alpha}\sqrt{LD}\omega} = \sqrt{\frac{\tau_p}{\rho_g} + \frac{K}{\alpha}\sqrt{2Lf_{cent}}} \tag{4}$$

The constants for the centrifugal effects have been determined from the STORM spinning disk experiment: $K_c = \left(\frac{We_D}{We_c}\right)^n$ with $n = 3$ and $We_c = 340000$ which is the critical Weber number below which the experimental results are dependent on the rim thickness. For the velocity contribution of the centrifugal effect, the factor $\alpha = 4.175$ was found (Dejean et al. [1]). Finally, for the constant K also used in Eq.(3), another database dealing with aerodynamics effects has to be used. It can be determined from literature, as for example from Chaussonnet et al. model for primary atomization [2] as shown in Dejean et al. [1]. In this paper, the model derived from the ONERA proprietary database for the secondary atomization has been used. This model was built in the very same manner as for the present model for centrifugation to take into account geometric and aerodynamics effects: several engine shapes were used with cases where aerodynamic effects can overcome reservoir effect (when the trailing edge is very thick for example).

4. Simulations tools

The CEDRE code is used to perform the simulations presented in this paper. CEDRE is ONERA's in-house CFD platform dedicated to multi-physics simulations. The code works on general unstructured meshes and couples several solvers dedicated to gas flow, particle trajectories and phase changes, radiation, wall liquid film…[4].

4.1 Implementation of the reemission model in CEDRE code

In the case of the Fan computation, three solvers are involved: CHARME, the Navier-Stokes solver to simulate the gas flow, SPARTE, the Lagrangian solver for the particles trajectories, and FILM, the Eulerian surface solver for the runback on the Fan walls (Figure 5).

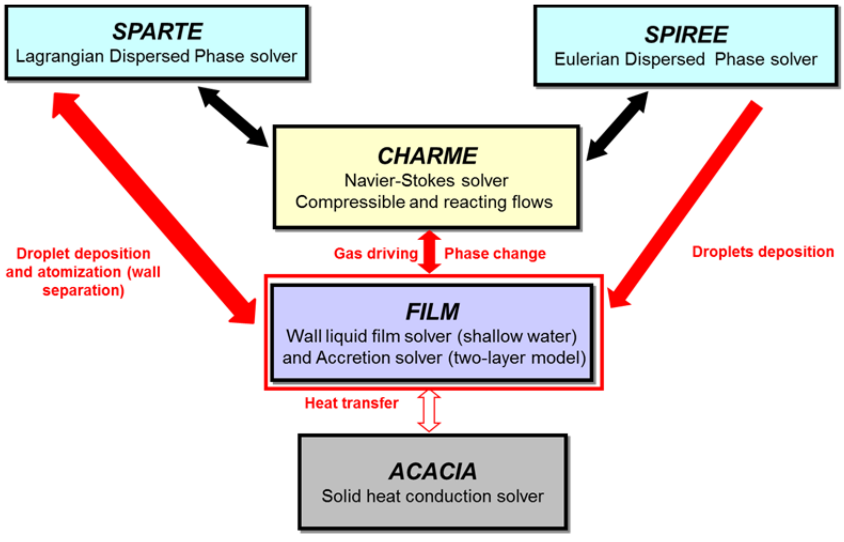

Figure 5: Coupling of FILM solver with other CEDRE solvers

The reemission model described in section 3 was implemented as a coupling procedure between the FILM solver and the SPARTE solver. The droplets are reinjected along boundaries of the FILM surface mesh when the model is activated. The weight of the numerical particles injected in the Lagrangian solver is determined by the runback liquid flow rate. The droplets are injected in dynamical and thermal equilibrium with the gas phase A refined mesh at the wall is required in order to accurately reproduce the droplets behaviour in the boundary layer. The diameters of the injected particles are specified via a random algorithm following a log-normal law. The scale parameter (variance) is set to a constant value obtained from ONERA's proprietary database. The D_{10} is given by the model and depends mainly on three parameters: the trailing edge thickness (specified by the user), the centrifugal force and the gas shear stress which are local values computed by the code. In order to be consistent with the model, the value of the gas shear stress has to be taken just before the trailing edge since it tends to drop significantly in the trailing edge wake.

Consequently, the user has to pay attention to the position of the FILM atomizing boundary. This step will be automated in the future to avoid any empiricism.

4.2 FILM solver

The FILM solver was first developed for the computation of wall liquid films formed in multi-physics applications involving a liquid phase and solid boundaries (see *Figure 6*). Recently, in the framework of the STORM project, it has been upgraded to a two-layer accretion model for icing simulations [5].

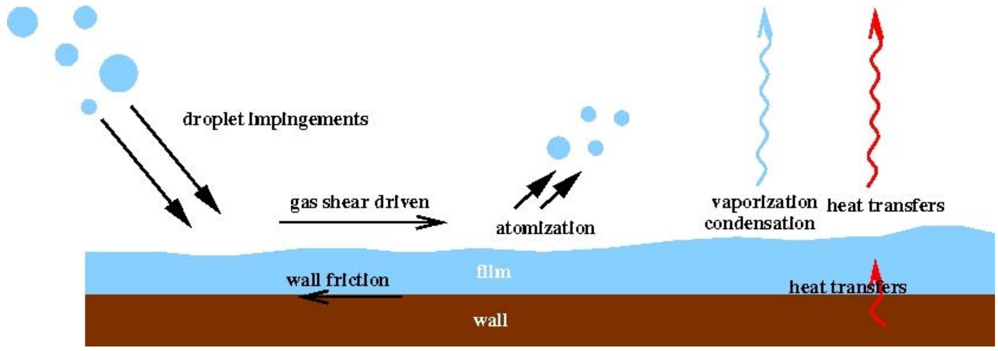

Figure 6: Models for runback in FILM solver

This solver uses a Eulerian approach to solve liquid film equations over a three dimensional surface. This kind of approach was successfully used by Foucard for automotive applications [6]. The liquid film equations are the Navier-Stokes equations integrated over the film thickness: the mass conservation, the momentum conservation and the energy conservation. In this paper, only the dynamic equations are solved. The Coriolis and the centrifugal forces are included in the momentum equation. For the dynamics, the system solved the so-called “two-equation model”, with one equation for the mass conservation and another equation for the momentum:

$$\frac{\partial \rho_l h_l}{\partial t} + div_t(\rho_l h_l \overline{\boldsymbol{v}}_{\boldsymbol{l}}) = \Phi_{imp,m,l} \quad \textbf{(5)}$$

$$\begin{aligned}\frac{\partial \rho_l h_l \overline{\boldsymbol{v}}_{\boldsymbol{l}}}{\partial t} &+ \boldsymbol{div_t}(\rho_l h_l \overline{\boldsymbol{v_l}.\boldsymbol{v_l}}) \\ &= -h_l \boldsymbol{grad_t}(p_g - \Phi_{imp,vn,l}) + \boldsymbol{\tau}_g + \boldsymbol{\Phi_{imp,vt,l}} + \rho_l \boldsymbol{g_t} h_l - \rho_l h_l(\boldsymbol{\omega} \wedge (\boldsymbol{\omega} \wedge \boldsymbol{r})) \\ &- 2\rho_l h_l(\boldsymbol{\omega} \wedge \overline{\boldsymbol{v}}_{\boldsymbol{l}}) + \boldsymbol{\tau}_w\end{aligned} \quad \textbf{(6)}$$

ρ_l is the liquid density, h_l the film thickness and $\overline{\boldsymbol{v}}_{\boldsymbol{l}}$ the mean velocity of the liquid film, tangential to the wall and integrated along the normal of the wall. Considering the liquid film to be very thin, the inertial term of the momentum equation is much lower than the source term, it is therefore assumed that $\overline{\boldsymbol{v_l}\boldsymbol{v_l}} \approx \overline{\boldsymbol{v}}_{\boldsymbol{l}}\overline{\boldsymbol{v}}_{\boldsymbol{l}}$ for the divergence term. $\Phi_{imp,m,l}$, $\Phi_{imp,vn,l}$ and $\boldsymbol{\Phi_{imp,vt,l}}$ denote the droplet impinging source terms, respectively for mass, normal momentum and tangential momentum. The other source terms in the momentum equation are the tangential gas pressure gradient $\boldsymbol{grad_t}(p_g)$, the gas shear stress $\boldsymbol{\tau}_g$, the tangential gravity $\boldsymbol{g_t}$ and the centrifugal and Coriolis forces for a rotating speed $\boldsymbol{\omega}$. The last term represents the friction coefficient on the wall $\boldsymbol{\tau}_w$. It is modelled supposing that the liquid film is locally at mechanical equilibrium yielding parabolic velocity profile within the film. Thus, this leads to the following wall constraint:

$$\boldsymbol{\tau_w} = \frac{3\mu_l(\overline{\boldsymbol{v}}_{\boldsymbol{l}} - \boldsymbol{v}_{\boldsymbol{l}}(0))}{h_l} - \frac{\boldsymbol{\tau_g} + \boldsymbol{\Phi_{imp,vt,l}}}{2} \quad \textbf{(7)}$$

The runback on the small scale Fan has thus been simulated using this set of equations.

DOI: 10.13009/EUCASS2017-517

5. Small scale Fan simulations

5.1 Geometry and definition of boundaries

Several tests were performed to define the influence of the boundary conditions. They highlight that the gas flow field is complex, especially in free ambient conditions. As it turns out to be more easy to simulate and as it happens to be more representative of realistic engines, the partially confined configuration was preferred. In this case, the geometry is made up of two domains: the Fan domain (rotating frame in red in Figure 7) and the downstream domain (fixed frame in green in Figure 7). The two domains are separated with a mixing plane discretized with 40 crowns. The configuration is partially confined (see Figure 1): the red domain is confined with a “wall” upper boundary condition whereas the green domain is not confined and the upper boundary condition is an “outlet”. Periodic boundary conditions are used to reduce the computational domain to a single blade.

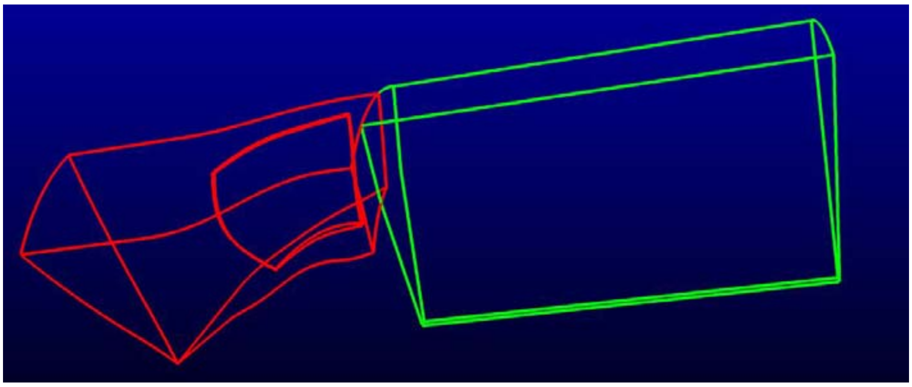

Figure 7: Simulated configuration

Then, regarding the boundary conditions for the liquid film, a specific issue concerning the surface geometry is the need to define a specific surface for the trailing edge (see section 4.1 and Figure 8). Indeed the droplets are reemitted at the boundaries of this surface and consequently the user needs to define the boundary conditions of the Fan (the procedure will be automated in the future).

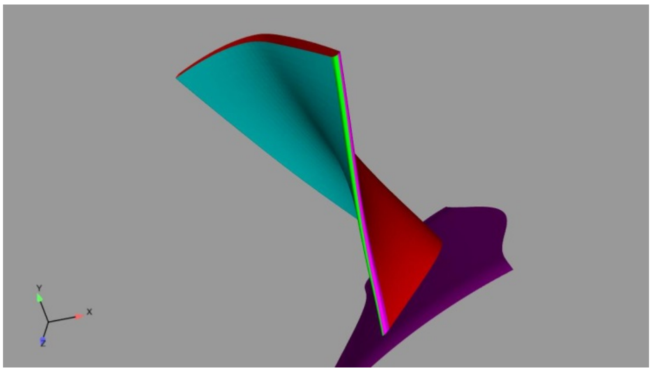

Figure 8: Fan geometry with a distinctive surface in the trailing edge for droplet reemission

5.2 Conditions retained

Two test-cases were computed. Both are partially confined (see section 5.1) and two rotational velocities were tested: 1000rpm (ie 105rad/s) and 2370rpm (ie 248rad/s).

For the gas phase simulations, a k-omega model was used with a turbulent rate of 1%. A low-Reynolds approach was used for the blades ($y^+ < 5$) whereas wall laws were used on the cone (larger mesh cells). Due to the difficulty to simulate the gas phase, several inlet and outlet boundary conditions were tested. Finally, the condition retained for the inlet is to impose a flow rate of 3.6kg.m^{-2}.s^{-1} in the 1000rpm case and of 6kg.m^{-2}.s^{-1} in the 2370 rpm case (these values are calculated from the gas velocity profiles plotted in Figure 4 and Figure 9) with a swirl respectively of -125kg.m^{-3}.rad.s^{-1} and -296 kg.m^{-3} (the swirl corresponds to the gas density multiplied by the rotation speed). Concerning the outlet condition, the pressure was imposed at 101325Pa.

DOI: 10.13009/EUCASS2017-517

Regarding the disperse phase, the inlet liquid flow rate was 175ml/min, which corresponds to a surface flow of 0.165kg.s^{-1}.m^{-2} calculated on a 150mm-diameter disk area. The droplets were injected using 100000 numerical particles with a uniform size distribution of 83µm (experimental D_{32}). This constitutes the primary droplet flow. For this first study, the injection conditions were simplified compared to the real ones (see Figure 3), the aim of this initial study being to understand the main phenomena.

5.3 Gas flow simulation

The first stage consisted in simulating the gas flow in the Fan and in the Downstream domains and validating the numerical results against the available experimental data. The velocity fields have been measured in the plane at 10mm downstream of the rear wall of the cone (see Figure 2 and Figure 9). The measurements show “bell curve” velocity profiles. In the 2370rpm case, the values are around two times greater than in the 1000rpm case, which is consistent with the physics. Another remarkable point is that the velocity is practically zero at the bottom of the measurement plane.

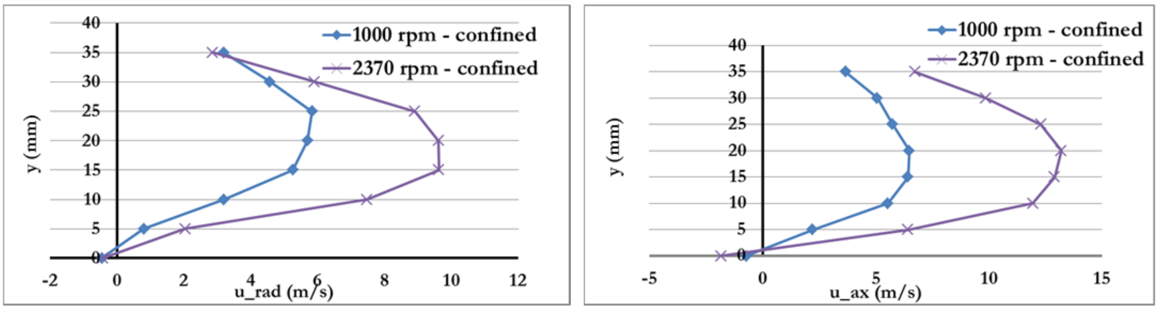

Figure 9: Axial and radial velocities measured in the plane 10mm behind the rear wall of the cone

However, in the CFD gas computations, due to the presence of a backward facing step downstream rear of the cone, wake vortices appear in the Downstream domain (see Figure 10) and the velocity profiles are not “bell curves”. In the 2370rpm case, the velocity field is roughly two times greater than in the 1000rpm case but the location of the wake is not the same: in the 2370rpm it is short and it goes down whereas in the 1000rpm case it is larger and more horizontal. Despite several tests, a better agreement with experimental measurements could not be achieved. Maybe the definition of the domains should be revised with “infinite” boundary conditions for better modelling the free ambient conditions.

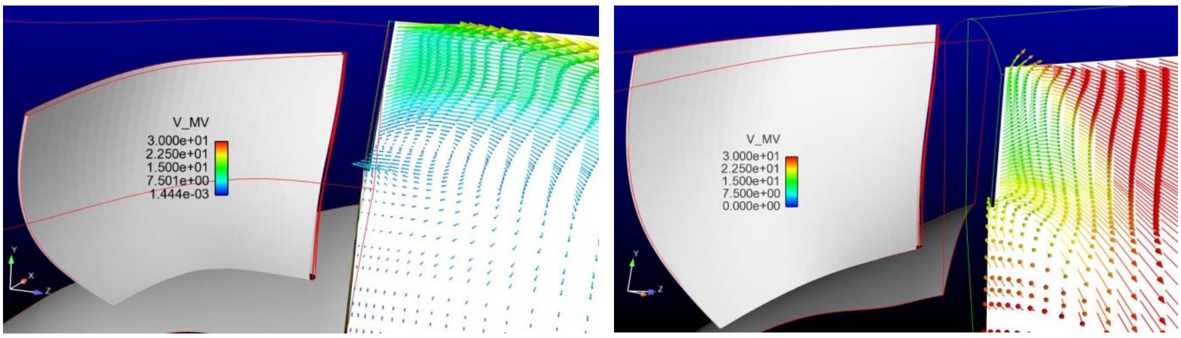

Figure 10: Gas simulation in downstream domain, gas velocity (left: 1000rpm, right: 2370rpm)

5.4 Disperse phase flow simulation

The simulations of droplet trajectories were performed using the Lagrangian solver SPARTE. A full deposition model was used for the droplet-wall interaction model since the classical wall interaction models are generally not validated for rotating wall conditions. The simulations have shown that some droplets are trapped in the gas recirculation zones and consequently the mass convergence threshold was set to 20%.
Figure 11 and Figure 12 show the droplet deposition on the hub and the blades. As expected, the droplets mainly impinge on the pressure side of the blade and on the hub. They also barely impinge on the suction side, just around the leading edge. In the 2370rpm case, the deposition zones are smaller than in the 1000rpm case, both on the cone

and on the blade. Moreover, in the 2370rpm case, droplets no longer cross the Fan: they are all trapped by the blade (see Figure 16). This explains why there is no more deposition at the rear of the blade since there are no longer droplets.

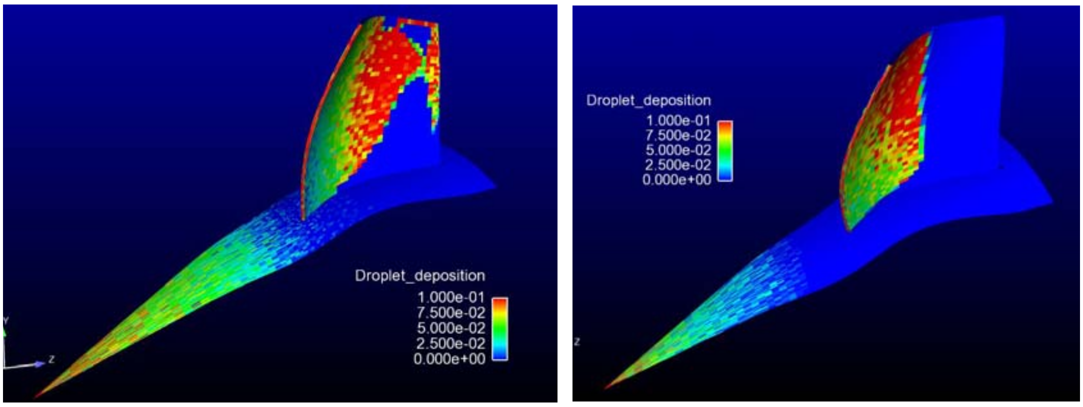

Figure 11: Droplet impingement on pressure side (left: 1000rpm, right: 2370rpm)

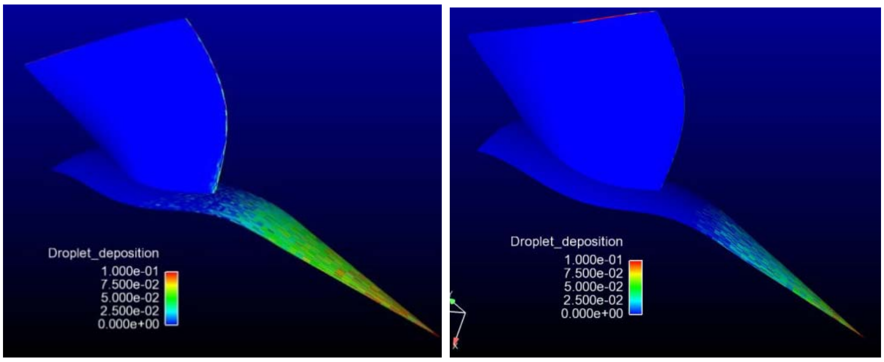

Figure 12: Droplet impingement on suction side (left: 1000rpm, right: 2370rpm)

5.5 Runback simulation

The runback on the walls was simulated using the FILM solver (see Figure 13 and Figure 14). On the cone, the liquid film is thicker in the 1000rpm case since the gas shear stress is lower compared to the 2370rpm case. For the blades, the spreading of the film is mainly determined by the centrifugation and the gas shear stress forces. On pressure side, the runback comes from direct droplet impingement whereas on the suction side, runback originates from the hub due to centrifugation.

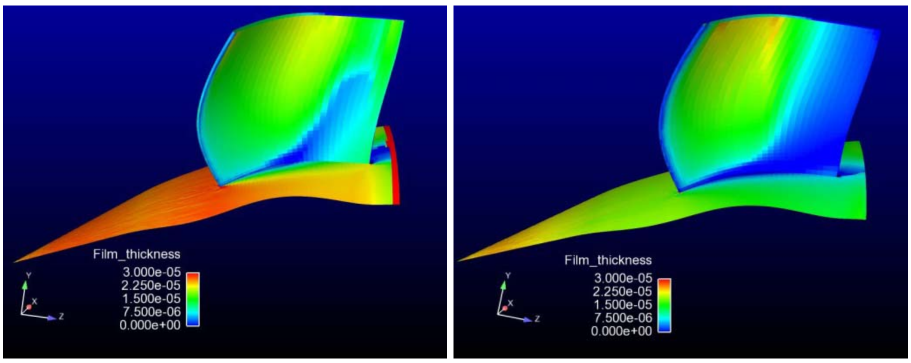

Figure 13: Runback on pressure side (left: 1000rpm, right: 2370rpm)

DOI: 10.13009/EUCASS2017-517

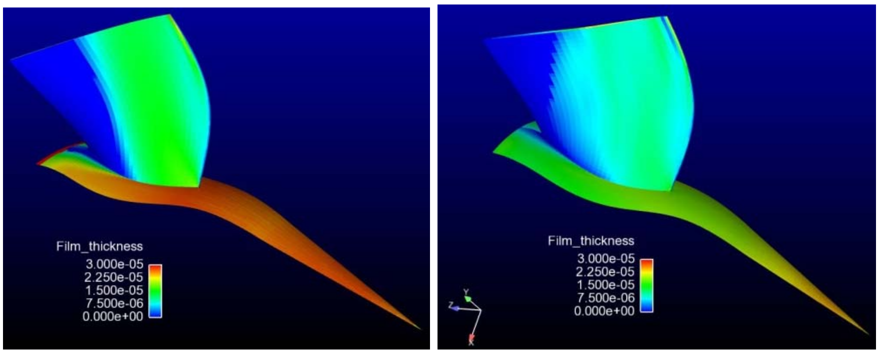

Figure 14: Runback on suction side (left: 1000rpm, right: 2370rpm)

These results can be qualitatively compared to the experimental visualizations presented in Table 3. A continuous liquid film appears on the cone. There is a transition to the rivulets regime before the blades. On the suction side, the water coming from the cone is centrifuged on the blade. However, on the pressure side, the water film is not clearly visible due to a weak reemitted light signal (see Figure 15). The authors assume that the water is spread on a thin continuous liquid film (around 20µm according to the simulations) without thicker rivulets.

The experimental visualizations highlight the existence of two runback regimes: continuous film and rivulets. The continuous liquid film approximation does not seem valid on the entire geometry. However, no rivulets model was available for the present computations. It would be worth using such a model to improve agreement with experimental data and this will be the object of future work. Nevertheless, note however that in the disk experiment, the reemitted droplets characteristics do not seem to depend on the film behaviour (Dejean et al. [1]).

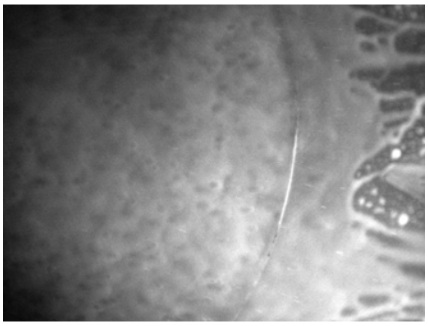	Cone	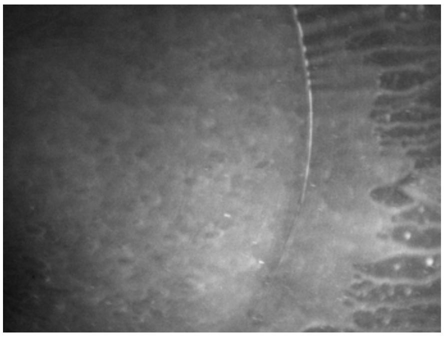
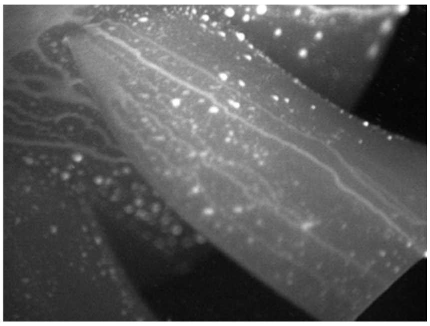	Suction side	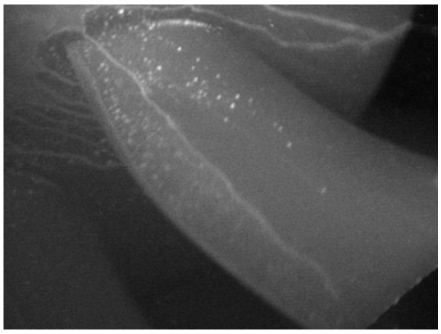
1000 rpm, 175 ml/min		2370 rpm, 175 ml/min

Table 3: Visualizations of the liquid behaviour on the Fan surfaces, liquid flow rate: 175 ml/min, non-confined case, comparisons between rotational velocities 1000rpm and 2370rpm

DOI: 10.13009/EUCASS2017-517

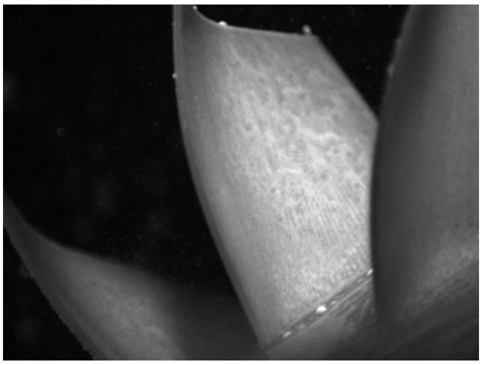

Figure 15: Liquid visualizations on the pressure side of the Fan blade

5.6 Droplets reemission simulation and validation

The computation of the reemitted droplets (secondary droplet flow) is performed using the SPARTE Lagrangian solver. The particles are injected in equilibrium with the gas phase along the boundaries of the trailing edge surface, defined by the user (see sections 4.1 and 5.1). Three injection points are positioned on each face of the boundary line and the size distribution function is discretized using 100 numerical particles. Figure 16 shows the centrifugal effect on the reemitted droplets. The bigger they are, the more they are centrifuged. Consequently the bigger particles do not cross the Mixing Plane.

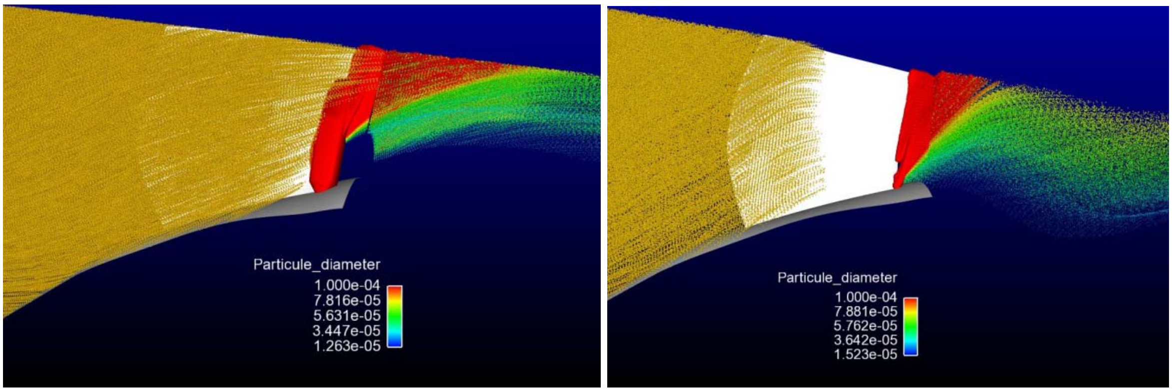

Figure 16: Droplet reemission [0:100µm] (left: 1000rpm, right: 2370rpm)

More over, it can be noticed that for the 2370rpm case, all the droplets are caught by the Fan. The experimental results measured in the plane 10mm behind the rear wall of the cone are presented in Figure 17. The Datarate curves show that a lot of droplets are trapped by the Fan (see lower Datarates at 1000rpm and 2370rpm compared to 0rpm). Concerning the 1000rpm case, there is a peak on the Datarate around 10mm position corresponding to a D_{32} of 79µm. The origin of this peak is unclear: primary droplets, secondary droplet flow or both? The value of the D_{32} and the value of the Datarate suggest it could be the primary droplet flow. However, this could be due to the reemission from the cone which is not taken into account in the simulations.

DOI: 10.13009/EUCASS2017-517

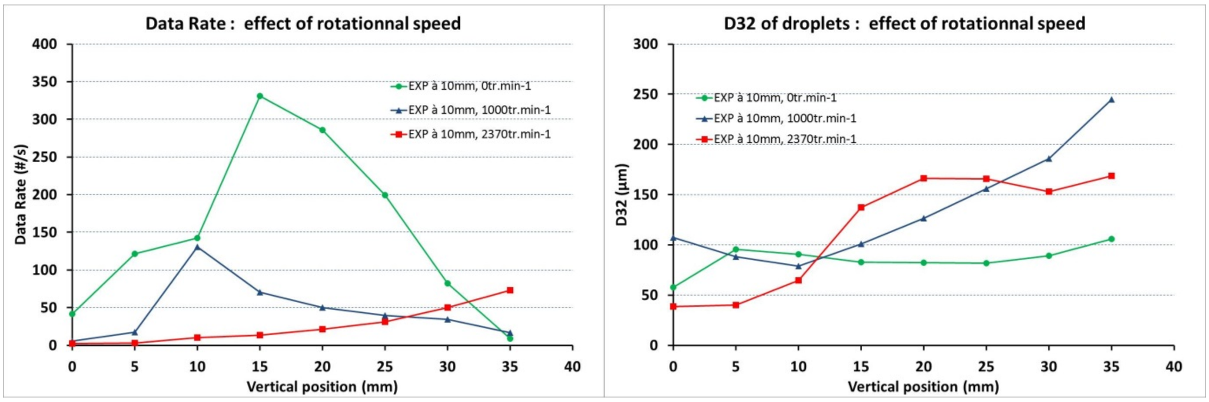

Figure 17: PDA droplet measurements in the plane 10mm behind the rear wall of the cone

In order to better understand the physical phenomena occurring behind the Fan, maps of D_{32} are plotted in different planes. Figure 18 is located just after the trailing edge and shows both primary and secondary droplets in the 1000rpm case but only the secondary droplets in the 2370rpm case. Figure 19 shows D_{32} in the experimental measurement plane 10mm behind the rear wall of the cone. The diameter values are averaged on each crown since the cut slice is located after the Mixing Plane. In order to analyse these results, the size volume distributions obtained with the PDA in this plane are plotted in Table 4, from the hub (bottom) to the shroud (top), for the 1000rpm case and 2370rpm case.

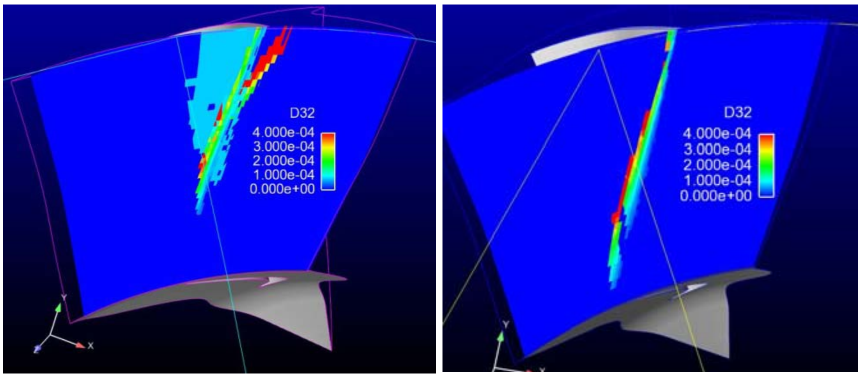

Figure 18 : D32 just after droplet reemission (z=1.5cm) [0:400µm], (left : 1000rpm, right : 2370rpm)

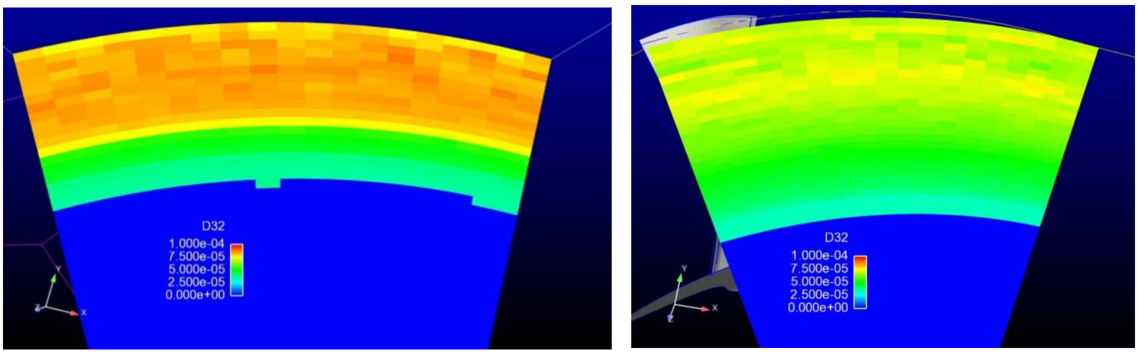

Figure 19 : D32 in the experimental measurement plane at 10mm from the rear wall of the cone (z=3.0cm) [0:100µm], (left : 1000rpm, right : 2370rpm)

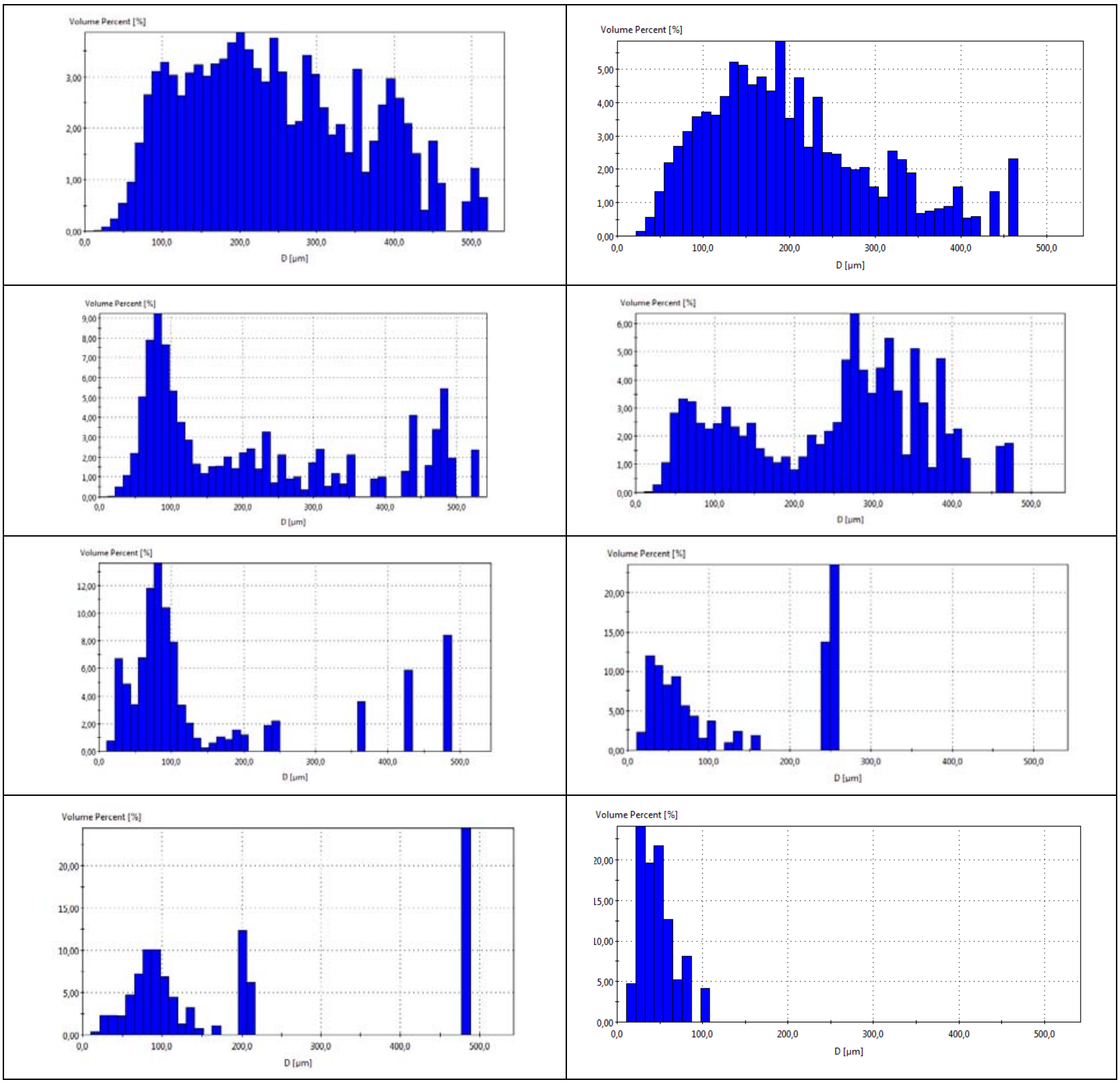

Table 4: Volume distribution of diameter in the experimental measurement plane at 10mm behind the rear wall of the cone (bottom) to the shroud (top) [0mm, 10mm, 20mm, 30mm] (left : 1000rpm, right : 2370rpm)

At the bottom in the 1000rpm case (left of Table 4), the distribution seems to be mainly composed of primary droplets (the experimental D_{32} is 83µm for the primary injected droplets) with also some larger droplets. These primary droplets appear in all histograms, from the bottom to the top, even if their volume percentage reduces due to the apparition of increasingly larger droplets. Considering the simulations, the assumption is made that these droplets originate from reemission at the Fan trailing edge. The centrifugation effect on the droplet trajectories explains that the volume distributions are filled up with larger droplets in the upward direction. In the 2370rpm case, the same tendency is observed, but without any primary droplets. Some smaller droplets appear at the bottom of the experimental plane.

Then, the experimental D_{32} is compared to the numerical values obtained in the measurement plane 10mm behind the rear wall of the cone (Figure 20). These results show that contrary to the experimental observations, there are no more droplets at the bottom of the measurement plane. Maybe, this effect is due to the presence of the wake vortices obtained in the gas numerical simulations (see Figure 10, a smaller vortex is observed in the 2370 case compared to the 1000rpm case). Then, it appears that the D_{32} obtained with the numerical simulations are smaller than in the experimental measurements. In order to understand if this discrepancy is due to the droplet reemission model or the computation of the droplet trajectories, the D_{32} of the droplet reemitted at the trailing edge is plotted in Figure 21. As expected, the droplet diameter of the reemitted droplets in the 2370rpm case is smaller than in the 1000rpm case. At the bottom of the blade, in the 1000rpm case, very large droplets are reemitted (with a D_{32} around 450µm). In fact,

DOI: 10.13009/EUCASS2017-517

due to a local recirculation (see red arrow at the bottom of the trailing edge in Figure 21), the gas shear stress is very small and the model thus predicts the generation of very large droplets.

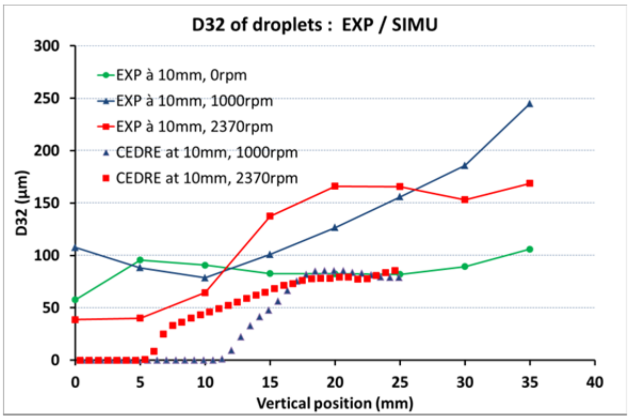

Figure 20 : Comparisons of experimental and numerical results on D_{32} on the experimental plane, 10mm behind the rear wall of the cone.

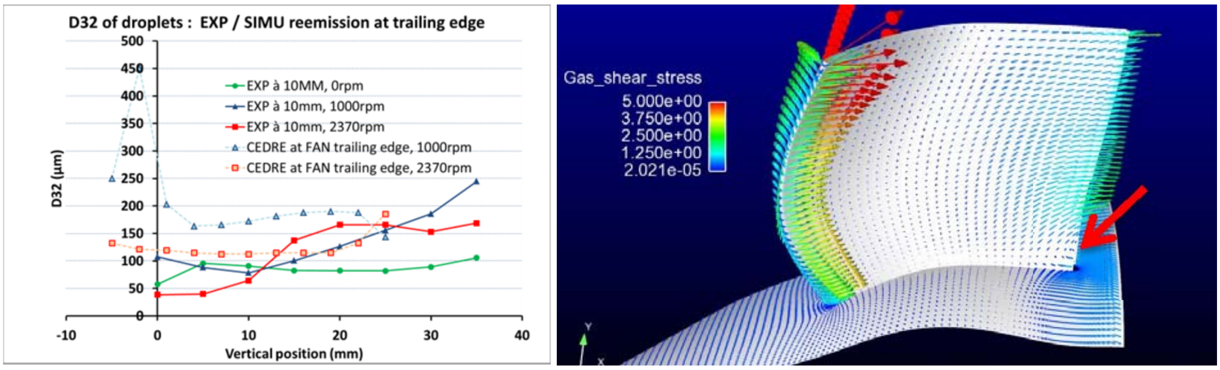

Figure 21 : Comparisons of experimental D_{32} and the numerical D_{32} of the reemitted droplets at the trailing edge of the blades.

However, at 10mm the D_{32} obtained in the numerical simulations in much smaller than the value computed at the trailing edge for the reemitted droplets. This significant centrifugal effect in numerical simulations is illustrated in Figure 22, where the D_{32} values are plotted in different planes. It shows centrifugation effect on droplet size, especially in the 1000rpm case where the largest reemitted droplets are removed before the Mixing Plane. More over, in the 1000rpm case, it should be noted that primary droplets are also crossing the measurement plane and consequently, the D_{32} value plotted in this case is not directly representative of reemitted droplets. This two effects entails that the results of 1000rpm case and 2370rpm case become closer. The same tendency seems visible for the experimental results but, at the top of the measurement plane, the droplets measured in the 1000rpm case remain larger.

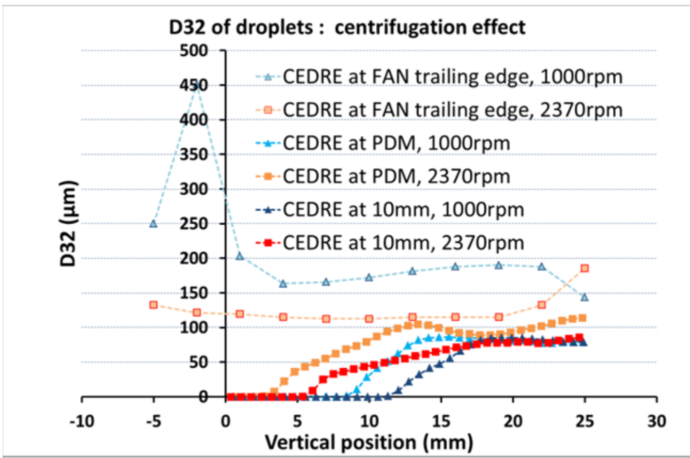

Figure 22: Comparisons of numerical results on D32

DOI: 10.13009/EUCASS2017-517

Finally, it is difficult to conclude whether the discrepancy between experimental and numerical results is due to a diameter underestimation of the reemitted droplets or an overestimation of the centrifugation effect. A critical point which was not investigated here is related to droplet injection . Indeed, academic studies on droplet atomization at the trailing edge showed that the injection velocity had a significant influence on the droplet trajectories back to the trailing edge. It would be interesting to further investigate this issue. Moreover, in order to validate the hypotheses made in this paper regarding droplet reemission phenomena, it would be necessary to perform a new experimental campaign providing local visualizations of reemission phenomena at the Fan trailing edge.

6. Conclusion

This paper presented the simulation of the runback on a small scale Fan experiment in order to validate the model of droplet reemission at the trailing edge in the context of the Appendix C icing conditions. The model was built from the coupling of two models: the first takes into account aerodynamic effect and geometry of the trailing edge on the reemitted droplets diameter and the other while the second models the centrifugal effect. Consequently, the objective of this paper was to validate the model on a configuration where both effects are acting simultaneously and on a configuration representative of a realistic engine. However, due to the significant scale reduction, the gas velocity was significantly lower that in a realistic application (around 10m/s instead of 100m/s). Gas simulations appeared to be quite complicated to perform due to the apparition of wake vortices behind the rear wall of the cone. Owing to these difficulties, only the partially confined configuration was simulated, with two different rotation velocities of the fan, 1000rpm and 2370rpm. A possible solution to overcome these difficulties could be to extend boundary conditions far away from the Fan model in order to better represent the free ambient conditions. The simulation of the runback of the wall liquid film and the droplet reemission was simulated with the CEDRE code. Regarding runback, , the presence of a liquid film on the suction side originating from the hub due to the centrifugation effects was noticed. These observations are in agreement with the present experiments. However, the simulations assume a continuous liquid film whereas rivulets are experimentally observed. Then, in the 2370rpm simulation test-case, all the droplets are trapped by the blade (impingement on the pressure side) whereas in the 1000rpm test-case some droplets are able to cross the Fan. The analysis of the experimental droplet distributions behind the Fan blades seems to validate this numerical result. At last, concerning the droplet mean diameters measured in the experimental plane behind the Fan, the centrifugal effect is experimentally well characterized since the droplet diameter roughly increases from bottom to top. However, the difference between the 1000rpm and the 2370rpm is not very pronounced. In the numerical results, the same tendency is observed in the measurement plane whereas at the trailing edge, the diameter of the reemitted droplets is larger in the 1000rpm case than in the 2370rpm case. Indeed, it appears numerically that the biggest droplets produced in the 1000rpm case are very rapidly centrifuged. Finally, the numerical droplet diameters obtained in the measurement plane are of the same order of magnitude but lower than in the experiments. Moreover, in the simulations, the droplets are only concentrated at the top of the plane, maybe due to the presence of gaseous recirculation zones. Finally, it is difficult to conclude if the discrepancy between numerical and experimental results on diameter comes from a deficiency of the model or from the droplet trajectories simulation. For this last point, it would seem important to investigate the injection of reemitted droplets since studies on more academic configurations have shown that the droplet trajectories are very sensitive to the injection velocity.

7. References

[1] Dejean, B., Radenac, E., Berthoumieu, P., 2016. Droplet reemission from rotating surfaces: experimental study on disks and a scale model Fan, and model derivation. In: *8th AIAA Atmospheric and Space Environments Conference, AIAA Aviation Forum, AIAA2016-3142*

[2] Chaussonnet, G., Vermorel, O., Riber, E., Cuenot, B., 2016. A new phenomenological model to predict drop size distribution in Large-Eddy Simulations of airblast atomizers *In: Int. J. Multiphase Flow 80:29-42*

[3] Frost, A.R., 1981. Rotary atomization in the ligament formation model. *In: T. Agric. Engng. Res. 26: 63-78*

[4] Refloch, A., Courbet, B., Murrone, A., Villedieu, P., Laurent, C., Gilbank, P., Troyes, J., Tessé, L., Chaineray, G., Dargaud, J.B., Quemerais, E. Vuillot, F., 2011. CEDRE Software, *In ; AerospaceLab 5, CFD Platforms and Coupling, ONERA*

[5] De Segura Solay, G. G., Radenac, E., Chauvin, R., Laurent, C, 2016. Simulations of ice accretion, runback and droplet re-emission in a multi-stage model of aeronautical engine, In: *8th AIAA Atmospheric and Space Environments Conference, AIAA Aviation Forum, AIAA2016-4350*

[6] Foucart, H., Habchi, C., Le Coz J.F., Baritaud T., 1998. Development of a three dimensional model of wall fuel liquid film for internal combustion engines, *In : SAE Transactions – J. of Engines 107*